

---

# Noise2Self: Blind Denoising by Self-Supervision

---

Joshua Batson<sup>1</sup> Loic Royer<sup>1</sup>

## Abstract

We propose a general framework for denoising high-dimensional measurements which requires no prior on the signal, no estimate of the noise, and no clean training data. The only assumption is that the noise exhibits statistical independence across different dimensions of the measurement. Moreover, our framework is not restricted to a particular denoising model. We show how it can be used to calibrate any parameterised denoising algorithm, from the single hyperparameter of a median filter to the millions of weights of a deep neural network. We demonstrate this on natural image and microscopy data, where we exploit noise independence between pixels, and on single-cell gene expression data, where we exploit independence between detections of individual molecules. Finally, we prove a theoretical lower bound on the performance of an optimal denoiser. This framework generalizes recent work on training neural nets from noisy images and on cross-validation for matrix factorization.

## 1. Introduction

We would often like to reconstruct a signal from high-dimensional measurements that are corrupted, under-sampled, or otherwise noisy. Devices like high-resolution cameras, electron microscopes, and DNA sequencers are capable of producing measurements in the thousands to millions of feature dimensions. But when these devices are pushed to their limits, taking videos with ultra-fast frame rates at very low-illumination, probing individual molecules with electron microscopes, or sequencing tens of thousands of cells simultaneously, each individual feature can become quite noisy. Nevertheless, the objects being studied are often very structured and the values of different features are highly correlated. Speaking loosely, if the “latent dimension” of the space of objects under study is much lower than

the dimension of the measurement, it may be possible to implicitly learn that structure, denoise the measurements, and recover the signal without any prior knowledge of the signal or the noise.

Traditional denoising methods each exploit a property of the noise, such as Gaussianity, or structure in the signal, such as spatiotemporal smoothness, self-similarity, or having low-rank. The performance of these methods is limited by the accuracy of their assumptions. For example, if the data are genuinely not low rank, then a low rank model will fit it poorly. This requires prior knowledge of the signal structure, which limits application to new domains and modalities. These methods also require calibration, as hyperparameters such as the degree of smoothness, the scale of self-similarity, or the rank of a matrix have dramatic impacts on performance.

In contrast, a data-driven prior, such as pairs  $(x_i, y_i)$  of noisy and clean measurements of the same target, can be used to set up a supervised learning problem. A neural net trained to predict  $y_i$  from  $x_i$  may be used to denoise new noisy measurements (Weigert et al., 2018). As long as the new data are drawn from the same distribution, one can expect performance similar to that observed during training. Lehtinen et al. demonstrated that clean targets are unnecessary (2018). A neural net trained on pairs  $(x_i, x'_i)$  of *independent* noisy measurements of the same target will, under certain distributional assumptions, learn to predict the clean signal. These supervised approaches extend to image denoising the success of convolutional neural nets, which currently give state-of-the-art performance for a vast range of image-to-image tasks. Both of these methods require an experimental setup in which each target may be measured multiple times, which can be difficult in practice.

In this paper, we propose a framework for blind denoising based on *self-supervision*. We use groups of features whose noise is independent conditional on the true signal to predict one another. This allows us to learn denoising functions from single noisy measurements of each target, with performance close to that of supervised methods. The same approach can also be used to calibrate traditional image denoising methods such as median filters and non-local means, and, using a different independence structure, denoise highly under-sampled single-cell gene expression data.

---

\*Equal contribution <sup>1</sup>Chan-Zuckerberg Biohub. Correspondence to: Joshua Batson <joshua.batson@czbiohub.org>, Loic Royer <loic.royer@czbiohub.org>.

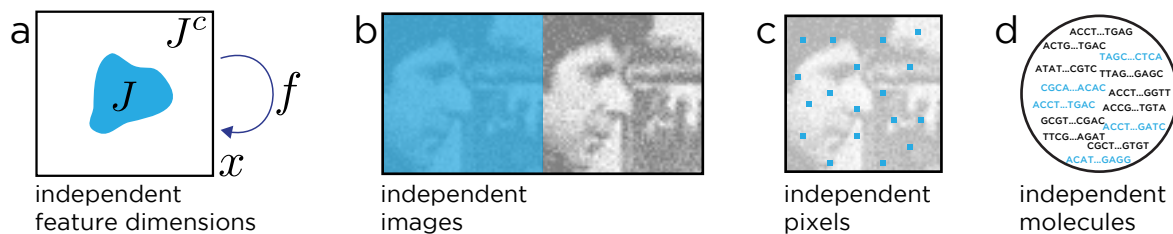


Figure 1. (a) The box represents the dimensions of the measurement  $x$ .  $J$  is a subset of the dimensions, and  $f$  is a  $J$ -invariant function: it has the property that the value of  $f(x)$  restricted to dimensions in  $J$ ,  $f(x)_J$ , does not depend on the value of  $x$  restricted to  $J$ ,  $x_J$ . This enables self-supervision when the noise in the data is conditionally independent between sets of dimensions. Here are 3 examples of dimension partitioning: (b) two independent image acquisitions, (c) independent pixels of a single image, (d) independently detected RNA molecules from a single cell.

We model the signal  $y$  and the noisy measurement  $x$  as a pair of random variables in  $\mathbb{R}^m$ . If  $J \subset \{1, \dots, m\}$  is a subset of the dimensions, we write  $x_J$  for  $x$  restricted to  $J$ .

**Definition.** Let  $\mathcal{J}$  be a partition of the dimensions  $\{1, \dots, m\}$  and let  $J \in \mathcal{J}$ . A function  $f: \mathbb{R}^m \rightarrow \mathbb{R}^m$  is  $J$ -invariant if  $f(x)_J$  does not depend on the value of  $x_J$ . It is  $\mathcal{J}$ -invariant if it is  $J$ -invariant for each  $J \in \mathcal{J}$ .

We propose minimizing the loss

$$\mathcal{L}(f) = \mathbb{E} \|f(x) - x\|^2, \quad (1)$$

over  $\mathcal{J}$ -invariant functions  $f$ . Since  $f$  has to use information from outside of each subset of dimensions  $J$  to predict the values inside of  $J$ , it cannot merely be the identity.

Suppose  $x$  is an unbiased estimator of  $y$ , that is,  $\mathbb{E}[x|y] = y$ , and the noise in each subset  $J \in \mathcal{J}$  is independent from the noise in its complement  $J^c$ , conditional on  $y$ . Then we can decompose the loss as

$$\mathcal{L}(f) = \mathbb{E} \|f(x) - y\|^2 + \mathbb{E} \|x - y\|^2, \quad (2)$$

the sum of the ordinary supervised loss and the variance of the noise. *By minimizing the self-supervised loss  $\mathcal{L}(f)$ , which we can compute from noisy data alone, we are able to find the actual optimal denoiser among any class of  $\mathcal{J}$ -invariant functions.*

For example, if the signal is an image with independent, mean-zero noise on each pixel, we may choose  $\mathcal{J} = \{\{1\}, \dots, \{m\}\}$  to be the singletons of each coordinate. In §3, we show how to adapt any traditional image denoising function into a  $\mathcal{J}$ -invariant one, and then calibrate it using this loss. For example, “donut” median filters, with a hole in the center, form a class of  $\mathcal{J}$ -invariant functions. By comparing the value of the loss for different filter radii, we are able to select the optimal radius for denoising the image at hand.

The donut median filter has just one parameter and therefore limited ability to adapt to the data. At the other extreme,

we may search over *all*  $\mathcal{J}$ -invariant functions for the global optimum:

**Proposition 1.** *The  $\mathcal{J}$ -invariant function  $f_{\mathcal{J}}^*$  minimizing (1) satisfies*

$$f_{\mathcal{J}}^*(x)_J = \mathbb{E}[y_J | x_{J^c}]$$

for each subset  $J \in \mathcal{J}$ .

That is, the optimal  $\mathcal{J}$ -invariant predictor for the dimensions of  $y$  in some  $J \in \mathcal{J}$  is their expected value conditional on observing the dimensions of  $x$  outside of  $J$ .

In §4, we use analytical examples to illustrate how the optimal  $\mathcal{J}$ -invariant denoising function approaches the optimal general denoising function as the amount of correlation between features in the data increases.

In practice, we may attempt to approximate the optimal denoiser by searching over a very large class of functions, such as deep neural networks with millions of parameters. In §5, we show that a deep convolutional network, modified to become  $\mathcal{J}$ -invariant using a masking procedure, can achieve state-of-the-art denoising performance on three diverse datasets.

Sample code is available on GitHub<sup>1</sup> and deferred proofs are contained in the Supplement.

## 2. Related Work

Each approach to blind denoising relies on assumptions about the structure of the signal and/or the noise. We review the major categories of assumption below, and the traditional and modern methods that utilize them. Most of the methods below are described in terms of application to image denoising, which has the richest literature, but some have natural extensions to other spatiotemporal signals and to generic measurements of vectors.

**Smoothness:** Natural images and other spatiotemporal signals are often assumed to vary smoothly (Buades et al.,

<sup>1</sup><https://github.com/czbiohub/noise2self>

2005b). Local averaging, using a Gaussian, median, or some other filter, is a simple way to smooth out a noisy input. The degree of smoothing to use, e.g., the width of a filter, is a hyperparameter often tuned by visual inspection.

**Self-Similarity:** Natural images are often self-similar, in that each patch in an image is similar to many other patches from the same image. The classic non-local means algorithm replaces the center pixel of each patch with a weighted average of central pixels from similar patches (Buades et al., 2005a). The more robust BM3D algorithm makes stacks of similar patches, and performs thresholding in frequency space (Dabov et al., 2007). The hyperparameters of these methods have a large effect on performance; the 12 hyperparameters of BM3D were set in the reference implementation by evaluating performance on a few images with simulated Gaussian noise (Lebrun, 2012). On a new dataset with an unknown noise distribution it is computationally expensive to evaluate different hyperparameter choices and difficult to evaluate their effects in a principled way.

Convolutional neural nets can produce images with another form of self-similarity, as linear combinations of the same small filters are used to produce each output. The “deep image prior” of (Ulyanov et al., 2017) exploits this by training a generative CNN to produce a single output image and stopping training before the loss goes to zero; the idea is that features shared in many places across the image are likely to be the signal, and will be learned before the net fits the noise.

**Generative:** Given a differentiable, generative model of the data, e.g. a neural net  $G$  trained using a generative adversarial loss, data can be denoised through projection onto the range of the net (Tripathi et al., 2018).

**Gaussianity:** Recent work (Zhussip et al., 2018; Metzler et al., 2018) uses a loss based on Stein’s unbiased risk estimator to train denoising neural nets in the special case that noise is i.i.d. Gaussian.

**Sparsity:** Natural images are often close to sparse in e.g. a wavelet or DCT basis (Chang et al., 2000). Compression algorithms such as JPEG exploit this feature by thresholding small transform coefficients (Pennebaker & Mitchell, 1992). This is also a denoising strategy, but artifacts familiar from poor compression (like the ringing around sharp edges) may occur. Hyperparameters include the choice of basis and the degree of thresholding. Other methods learn an overcomplete dictionary from the data (Elad & Aharon, 2006; Pappayan et al., 2017), and seek sparsity in that basis.

**Compressibility:** A generic approach to denoising is to lossily compress and then decompress the data. The accuracy of this approach depends on the applicability of the compression scheme used to the signal at hand and its robustness to the form of noise. It also depends on choosing

the degree of compression correctly: too much will lose important features of the signal, too little will preserve all of the noise. For the sparsity methods, this “knob” is the degree of sparsity, while for low-rank matrix factorizations, it is the rank of the matrix.

Autoencoder architectures for neural nets provide a general framework for learnable compression. Each sample is mapped to a low-dimensional representation—the value of the neural net at the bottleneck layer— then back to the original space (Gallinari et al., 1987; Vincent et al., 2010). An autoencoder trained on noisy data may produce cleaner data as its output. The degree of compression is determined by the width of the bottleneck layer.

UNet architectures, in which skip connections are added to a typical autoencoder architecture, can capture high-level spatially coarse representations and also reproduce fine detail; they can, in particular, learn the identity function (Ronneberger et al., 2015). Trained directly on noisy data, they will do no denoising. Trained with clean targets, they can learn very accurate denoising functions (Weigert et al., 2018).

**Statistical Independence:** Lehtinen et al. observed that a UNet trained to predict one noisy measurement of a signal from an independent noisy measurement of the same signal will in fact learn to predict the true signal (Lehtinen et al., 2018). We may reformulate the Noise2Noise procedure in terms of  $\mathcal{J}$ -invariant functions: if  $x_1 = y + n_1$  and  $x_2 = y + n_2$  are the two measurements, we consider the composite measurement  $x = (x_1, x_2)$  of a composite signal  $(y, y)$  in  $\mathbb{R}^{2m}$  and set  $\mathcal{J} = \{J_1, J_2\} = \{\{1, \dots, m\}, \{m + 1, \dots, 2m\}\}$ . Then  $f_{\mathcal{J}}^*(x)_{J_2} = \mathbb{E}[y|x_1]$ .

An extension to video, in which one frame is used to compute the pullback under optical flow of another, was explored in (Ehret et al., 2018).

In concurrent work, Krull et al. describe an approach for learning to denoise from single noisy images with independent noise on each pixel (2018). They train a UNet to predict a collection of held-out pixels of an image from a version of that image with those pixels replaced. A key difference between their approach and our neural net examples in §5 is in that their replacement strategy is not quite  $\mathcal{J}$ -invariant. (With some probability a given pixel is replaced by itself.) While their method lacks a theoretical guarantee against fitting the noise, it performs well in practice: On synthetically noised natural and microscopy images, they show performance similar to supervised methods, and on real cryo-TEM and fluorescence microscopy data, they show increased contrast and reduced speckle noise.

Finally, we note that the “fully emphasized denoising autoencoders” in (Vincent et al., 2010) used the MSE between an autoencoder evaluated on masked input data and the true

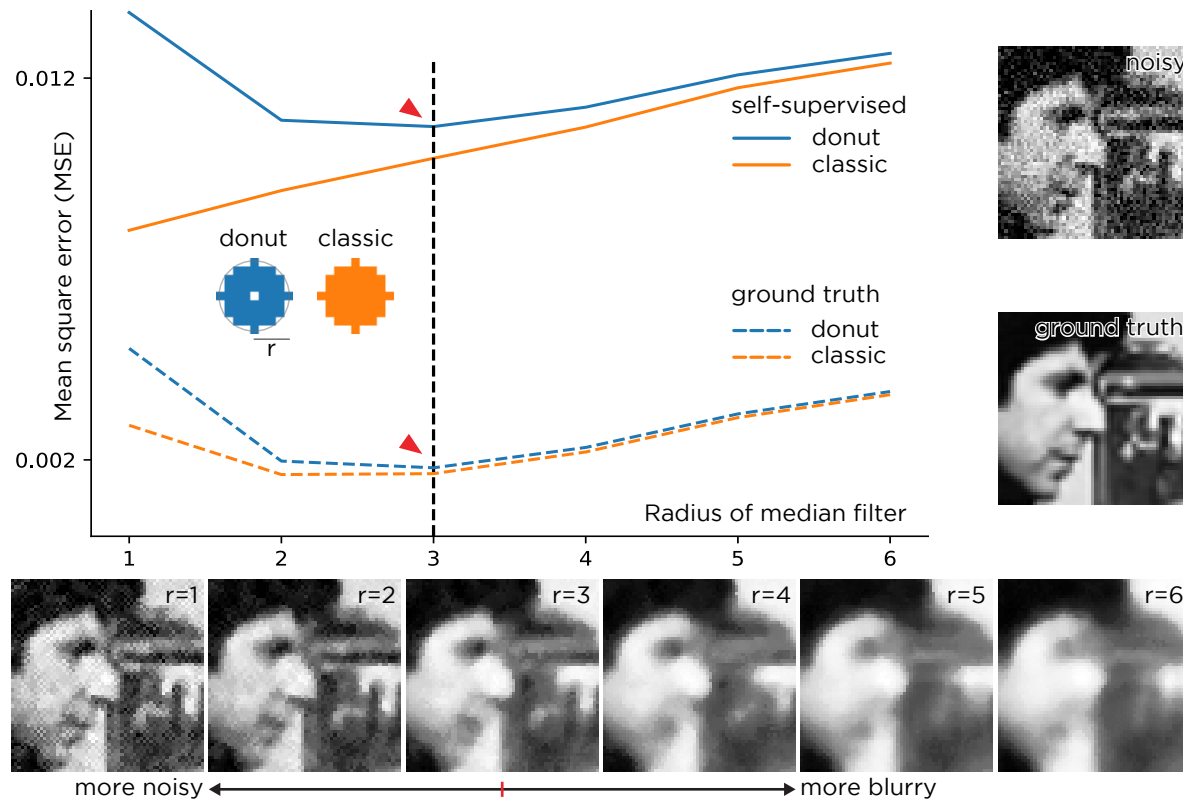


Figure 2. Calibrating a median filter without ground truth. Different median filters may be obtained by varying the filter’s radius. Which is optimal for a given image? The optimal parameter for  $\mathcal{J}$ -invariant functions such as the donut median can be read off (red arrows) from the self-supervised loss.

value of the masked pixels, but with the goal of learning robust representations, not denoising.

### 3. Calibrating Traditional Models

Many denoising models have hyperparameters controlling the extent or scale of the denoising—the size of a filter, the threshold for sparsity, the number of principal components, the width of a bottleneck. If ground truth data were available, the optimal parameter  $\theta$  for a family  $f_\theta$  could be chosen by minimizing  $\|f_\theta(x) - y\|^2$ .

In this section, we show how to make any traditional denoising function  $f_\theta$  into a  $\mathcal{J}$ -invariant model  $g_\theta$ , whose optimal parameters can be found by minimizing the loss  $\mathcal{L}(g_\theta) = \|g_\theta(x) - x\|^2$ .

We illustrate this process in Figure 2 for the median filter  $f_r$ , which replaces each pixel with the median over a disk of radius  $r$  surrounding it. We consider an image with i.i.d. Gaussian noise, and let  $\mathcal{J} = \{\{1\}, \dots, \{m\}\}$  be the partition into single pixels. The  $\mathcal{J}$ -invariant function is the “donut” median  $g_r$ , which replaces each pixel with the median over the same disk *excluding the center*. For the

donut median, the minimum of the function  $\|g_r(x) - x\|^2$  (solid blue) sits directly above the minimum of the true reconstruction error  $\|g_r(x) - y\|^2$  (dashed blue), and selects the optimal radius  $r = 3$ . In contrast, the function  $\|f_r(x) - x\|^2$  (solid orange) is strictly increasing and tells us nothing about the true reconstruction error  $\|f_r(x) - y\|^2$  (dashed orange). Note that the median and donut median are genuinely different functions with slightly different performance, but while the former can only be tuned by inspecting the output images, the latter can be tuned using a principled loss.

More generally, let  $f_\theta$  be a classical denoiser, and consider some partition  $\mathcal{J}$  of the pixels. Let  $s(x)$  be the function replacing each pixel with the average of its neighbors. Then the function  $g_\theta$  defined by

$$g_\theta(x)_J := f_\theta(\mathbf{1}_J \cdot s(x) + \mathbf{1}_{J^c} \cdot x)_J, \quad (3)$$

for each  $J \in \mathcal{J}$ , is  $\mathcal{J}$ -invariant.

In Supp. Figure 1, we show the corresponding loss curves for a wavelet filter, where we tune the threshold  $\sigma$ , and NL-means, where we tune a cut-off distance  $h$  (Buades et al., 2005a; Chang et al., 2000). The partition  $\mathcal{J}$  used is

Table 1. Comparison of optimally tuned  $\mathcal{J}$ -invariant versions of classical denoising models. PSNR+ denotes the small performance boost from including an optimal amount of the noisy input (§4.2)

METHOD	LOSS	PSNR	PSNR+
(DONUT) MEDIAN	0.0107	27.5	28.2
WAVELET	0.0113	26.0	26.9
NL-MEANS	<b>0.0098</b>	<b>30.4</b>	<b>30.8</b>

a 4x4 grid. Note that in all these examples, the function  $g_\theta$  is genuinely different than  $f_\theta$ , and, because the simple interpolation procedure may itself be helpful, it sometimes performs better.

In Table 1, we use the same loss to compare all three classes of denoising function. It selects the NL-means reconstruction as the best. Remarkably, this tuning process can be done on individual noisy images.

### 3.1. Single-Cell

In single-cell transcriptomic experiments, thousands of individual cells are isolated, lysed, and their mRNA are extracted, barcoded, and sequenced. Each mRNA molecule is mapped to a gene, and that  $\sim 20,000$ -dimensional vector of counts is an approximation to the gene expression of that cell. In modern, highly parallel experiments, only a few thousand of the hundreds of thousands of mRNA molecules present in a cell are successfully captured and sequenced (Milo et al., 2010). Thus the expression vectors are very undersampled, and genes expressed at low levels will appear as zeros. This makes simple relationships among genes, such as co-expression or transitions during development, difficult to see.

If we think of the measurement as a set of molecules captured from a given cell, then we may partition the molecules at random into two sets  $J_1$  and  $J_2$ . Summing (and normalizing) the gene counts in each set produces expression vectors  $x_{J_1}$  and  $x_{J_2}$  which are independent conditional on the true mRNA content  $y$ . We may now attempt to denoise  $x$  by training a model to predict  $x_{J_2}$  from  $x_{J_1}$  and vice versa.

We demonstrate this on a dataset of 2730 bone marrow cells from Paul et al. using principal component regression (Paul et al., 2015), where we use the self-supervised loss to find an optimal number of principal components. The data contain a population of stem cells which differentiate either into erythroid or myeloid lineages. The expression of genes preferentially expressed in each of these cell types is shown in Figure 3 for both the (normalized) noisy data and data denoised with too many, too few, and an optimal number of principal components. In the raw data, it is difficult to discern any population structure. When the data is under-corrected, the stem cell marker *Ifitm1* is still not

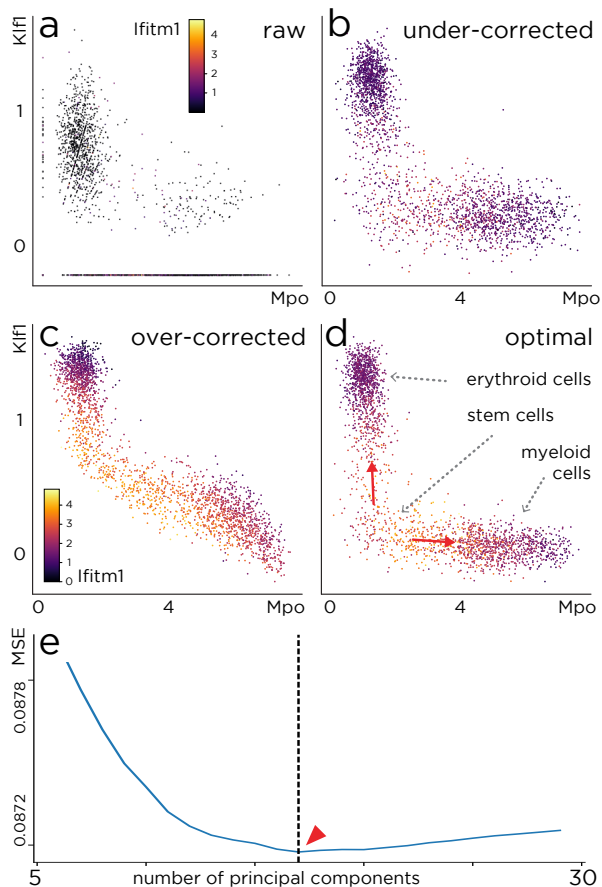


Figure 3. Self-supervised loss calibrates a linear denoiser for single cell data. (a) Raw expression of three genes: a myeloid cell marker (Mpo), an erythroid cell marker (Klf1), and a stem cell marker (Ifitm1). Each point corresponds to a cell. (e) Self-supervised loss for principal component regression. In (d) we show the denoised data for the optimal number of principal components (17, red arrow). In (c) we show the result of using too few components and in (b) that of using too many. X-axes show square-root normalised counts.

visible. When it is over-corrected, the stem population appears to express substantial amounts of *Klf1* and *Mpo*. In the optimally corrected version, *Ifitm1* expression coincides with low expression of the other markers, identifying the stem population, and its transition to the two more mature states is easy to see.

### 3.2. PCA

Cross-validation for choosing the rank of a PCA requires some care, since adding more principal components will always produce a better fit, even on held-out samples (Bro et al., 2008). Owen and Perry recommend splitting the feature dimensions into two sets  $J_1$  and  $J_2$  as well as splitting the samples into train and validation sets (Owen & Perry, 2009). For a given  $k$ , they fit a rank  $k$  princi-

pal component regression  $f_k : X_{\text{train}, J_1} \mapsto X_{\text{train}, J_2}$  and evaluate its predictions on the validation set, computing  $\|f_k(X_{\text{valid}, J_1}) - X_{\text{valid}, J_2}\|^2$ . They repeat this, permuting train and validation sets and  $J_1$  and  $J_2$ . Simulations show that if  $X$  is actually a sum of a low-rank matrix plus Gaussian noise, then the  $k$  minimizing the total validation loss is often the optimal choice (Owen & Perry, 2009; Owen et al., 2016). This calculation corresponds to using the self-supervised loss to train and cross-validate a  $\{J_1, J_2\}$ -invariant principal component regression.

## 4. Theory

In an ideal situation for signal reconstruction, we have a prior  $p(y)$  for the signal and a probabilistic model of the noisy measurement process  $p(x|y)$ . After observing some measurement  $x$ , the posterior distribution for  $y$  is given by Bayes' rule:

$$p(y|x) = \frac{p(x|y)p(y)}{\int p(x|y)p(y)dy}.$$

In practice, one seeks some function  $f(x)$  approximating a relevant statistic of  $y|x$ , such as its mean or median. The mean is provided by the function minimizing the loss:

$$\mathbb{E}_x \|f(x) - y\|^2$$

(The  $L^1$  norm would produce the median) (Murphy, 2012).

Fix a partition  $\mathcal{J}$  of the dimensions  $\{1, \dots, n\}$  of  $x$  and suppose that for each  $J \in \mathcal{J}$ , we have

$$p(x|y) = p(x_J|y)p(x_{J^c}|y),$$

i.e.,  $x_J$  and  $x_{J^c}$  are independent conditional on  $y$ . We consider the loss

$$\mathbb{E}_x \|f(x) - x\|^2 = \mathbb{E}_{x,y} \|f(x) - y\|^2 + \|x - y\|^2 - 2\langle f(x) - y, x - y \rangle$$

If  $f$  is  $\mathcal{J}$ -invariant, then  $f(x)_j$  and  $x_j$  are independent random variables for all  $j$ , and the third term reduces to  $\mathbb{E}_y \langle \mathbb{E}_{x|y}[f(x) - y], \mathbb{E}_{x|y}[x - y] \rangle$ , which vanishes when  $x$  is an unbiased estimator of  $y$ . (This is Proposition 1.)

Any  $\mathcal{J}$ -invariant function can be written as a collection of ordinary functions  $f_J : \mathbb{R}^{|J^c|} \rightarrow \mathbb{R}^{|J|}$ , where we separate the output dimensions of  $f$  based on which input dimensions they depend on. Then

$$\mathcal{L}(f) = \sum_{J \in \mathcal{J}} \mathbb{E} \|f_J(x_{J^c}) - x_J\|^2.$$

This is minimized at

$$f_J^*(x_{J^c}) = \mathbb{E}[x_J|x_{J^c}] = \mathbb{E}[y_J|x_{J^c}].$$

We bundle these functions into  $f_{\mathcal{J}}^*$ .

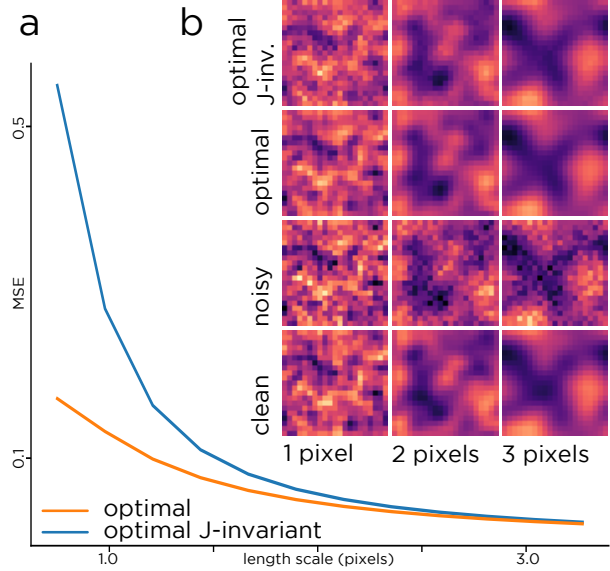


Figure 4. The optimal  $\mathcal{J}$ -invariant predictor converges to the optimal predictor. Example images for Gaussian processes of different length scales. We show how the gap in image quality between the two predictors tends to zero as the length scale increases.

### 4.1. How good is the optimum?

How much information do we lose by giving up  $x_J$  when trying to predict  $y_J$ ? Roughly speaking, the more the features in  $J$  are correlated with those outside of it, the closer  $f_{\mathcal{J}}^*(x)$  will be to  $\mathbb{E}[y|x]$  and the better both will estimate  $y$ .

Figure 4 illustrates this phenomenon for the example of Gaussian Processes, a computationally tractable model of signals with correlated features. We consider a process on a  $33 \times 33$  toroidal grid. The value of  $y$  at each node is standard normal and the correlation between the values at  $p$  and  $q$  depends on the distance between them:  $K_{p,q} = \exp(-\|p - q\|^2 / 2\ell^2)$ , where  $\ell$  is the length scale. The noisy measurement  $x = y + n$ , where  $n$  is white Gaussian noise with standard deviation 0.5.

While

$$\mathbb{E}\|y - f_{\mathcal{J}}^*(x)\|^2 \geq \mathbb{E}\|y - \mathbb{E}[y|x]\|^2$$

for all  $\ell$ , the gap decreases quickly as the length scale increases.

The Gaussian process is more than a convenient example; it actually represents a worst case for the recovery error as a function of correlation.

**Proposition 2.** *Let  $x, y$  be random variables and let  $x^G$  and  $y^G$  be Gaussian random variables with the same covariance matrix. Let  $f_{\mathcal{J}}^*$  and  $f_{\mathcal{J}}^{*,G}$  be the corresponding optimal  $\mathcal{J}$ -invariant predictors. Then*

$$\mathbb{E}\|y - f_{\mathcal{J}}^*(x)\|^2 \leq \mathbb{E}\|y - f_{\mathcal{J}}^{*,G}(x)\|^2.$$

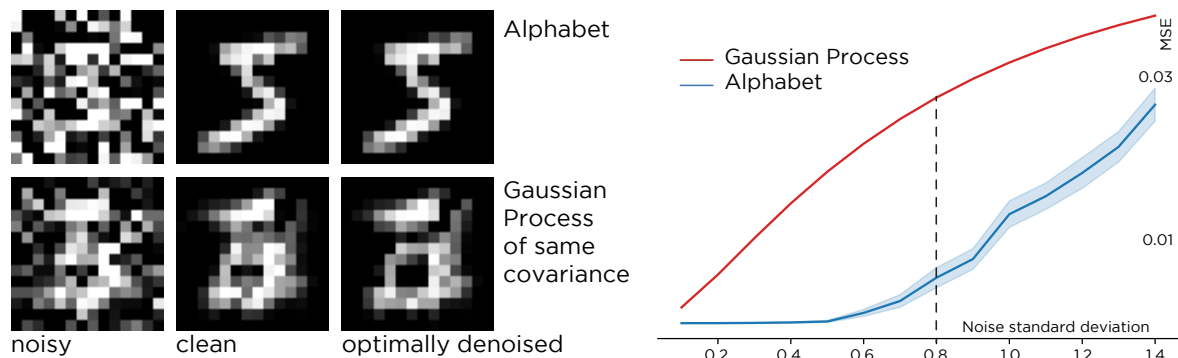


Figure 5. For any dataset, the error of the optimal predictor (blue) is lower than that for a Gaussian Process (red) with the same covariance matrix. We show this for a dataset of noisy digits: the quality of the denoising is visibly better for the Alphabet than the Gaussian Process (samples at  $\sigma = 0.8$ ).

*Proof.* See Supplement.  $\square$

Gaussian processes represent a kind of local texture with no higher structure, and the functions  $f_{\mathcal{J}}^*$  turn out to be linear (Murphy, 2012).

At the other extreme is data drawn from finite collection of templates, like symbols in an alphabet. If the alphabet consists of  $\{a_1, \dots, a_r\} \in \mathbb{R}^m$  and the noise is i.i.d. mean-zero Gaussian with variance  $\sigma^2$ , then the optimal  $\mathcal{J}$ -invariant prediction independent is a weighted sum of the letters from the alphabet. The weights

$$w_i = \exp(-\|(a_i - x) \cdot \mathbf{1}_{\mathcal{J}^c}\|^2 / 2\sigma^2)$$

correspond to the posterior probabilities of each letter. When the noise is low, the output will concentrate on a copy of the closest letter; when the noise is high, the output will be the average of many letters.

In Figure 5, we demonstrate this phenomenon for an alphabet consisting of 30 16x16 handwritten digits drawn from MNIST (LeCun et al., 1998). Note that almost exact recovery is possible at much higher levels of noise than the Gaussian process with covariance matrix given by the empirical covariance matrix of the alphabet.

Any real-world datasets will exhibit more structure than a Gaussian process, so nonlinear functions can generate significantly better predictions.

#### 4.2. Doing better

If  $f$  is  $\mathcal{J}$ -invariant, then by definition  $f(x)_j$  contains no information from  $x_j$ , and the right linear combination  $\lambda f(x)_j + (1 - \lambda)x_j$  will produce an estimate of  $y_j$  with lower variance than either. The optimal value of  $\lambda$  can be computed from the variance of the noise, if known. The performance gain depends on the quality of  $f$ : for example, if  $f$  improves the PSNR by 10 dB, then mixing in the optimal

amount of  $x$  will yield another 0.4 dB. (See Table 1 for an example and Supplement for proofs.)

## 5. Deep Learning Denoisers

The self-supervised loss can also be used to train deep convolutional neural nets from single samples of noisy images. We show this on three datasets from different domains (see Figure 6) with strong synthetic noise applied independently to each pixel. We use a UNet architecture and a random partition of 25 subsets for  $\mathcal{J}$ . We make the neural net  $\mathcal{J}$ -invariant as in Eq. 3, except we replace the masked pixels with random values instead of local averages.

As shown in Table 2, we achieve superior performance to the classic unsupervised denoisers NLM and BM3D, and comparable performance to the same architecture trained with clean targets (Noise2Truth) and with independently noisy targets (Noise2Noise), and to a purely convolutional architecture with clean targets (DnCNN) (Zhang et al., 2017).

The result of training is a neural net  $f_{\theta}$ , which, when converted into a  $\mathcal{J}$ -invariant function  $g_{\theta}$ , has low self-supervised loss. We found that applying  $f_{\theta}$  directly to the noisy input gave slightly better (0.5 dB) performance than using  $g_{\theta}$ . The images in Figure 6 correspond to applying  $f_{\theta}$ .

Experiments were performed on a single NVIDIA Titan XP GPU.

## 6. Discussion

We have demonstrated a general framework for denoising high-dimensional measurements whose noise exhibits some conditional independence structure. We have shown how to use a self-supervised loss to calibrate or train any  $\mathcal{J}$ -invariant class of denoising functions.

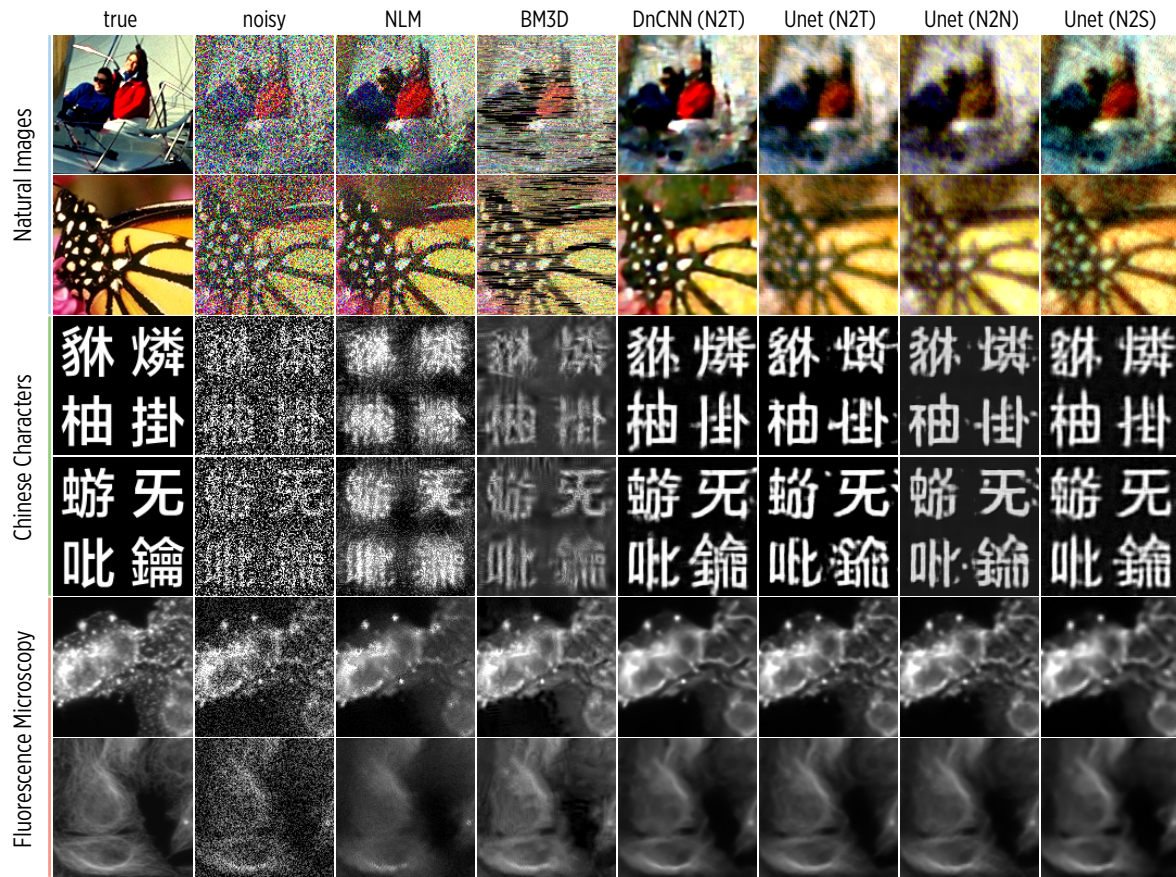


Figure 6. Benchmarking of classic, supervised, and self-supervised denoising methods on natural images, Chinese characters, and fluorescence microscopy images. Baseline denoisers are: NLM (Buades et al., 2005a), BM3D (Dabov et al., 2007), and a supervised CNN-based denoiser, DnCNN (Zhang et al., 2017). We compare denoising performance of a UNet trained with three losses: supervised with truth (N2T), supervised with another noisy image (N2N), and self-supervised (N2S).

Table 2. Comparison of different denoising models and training modalities. We compare the Peak Signal to Noise Ratio (PSNR) on held-out test data. Error bars from training five models.

METHOD	HÀNZÌ	IMAGENET	CELLNET
RAW	6.5	9.4	15.1
NLM	8.4	15.7	29.0
BM3D	9.3	15.5	31.4
DnCNN (N2T)	14.0 ± 0.1	22.0	34.4 ± 0.1
UNET (N2T)	13.1 ± 0.7	21.1	34.5 ± 0.1
UNET (N2N)	13.3 ± 0.5	17.8	34.4 ± 0.1
UNET (N2S)	13.8 ± 0.3	18.6	32.8 ± 0.2

There remain many open questions about the optimal choice of partition  $\mathcal{J}$  for a given problem. The structure of  $\mathcal{J}$  must reflect the patterns of dependence in the signal and independence in the noise. The relative sizes of each subset  $J \in \mathcal{J}$  and its complement creates a bias-variance tradeoff in the

loss, exchanging information used to make a prediction for information about the quality of that prediction.

For example, the measurements of single-cell gene expression could be partitioned by molecule, gene, or even pathway, reflecting different assumptions about the kind of stochasticity occurring in transcription.

We hope this framework will find application to other domains, such as sensor networks in agriculture or geology, time series of whole brain neuronal activity, or telescope observations of distant celestial bodies.

## Acknowledgements

Thank you to James Webber, Jeremy Freeman, David Dynerman, Nicholas Sofroniew, Jaakko Lehtinen, Jenny Folkesson, Anitha Krishnan, and Vedran Hadziosmanovic for valuable conversations. Thank you to Jack Kamm for discussions on Gaussian Processes and shrinkage estimators.

Thank you to Martin Weigert for his help running BM3D. Thank you to the Chan Zuckerberg Biohub for financial support.

## References

- Bro, R., Kjeldahl, K., Smilde, A. K., and Kiers, H. A. L. Cross-validation of component models: A critical look at current methods. *Analytical and Bioanalytical Chemistry*, 390(5):1241–1251, March 2008. ISSN 1618-2642, 1618-2650. doi: 10.1007/s00216-007-1790-1. URL <http://link.springer.com/10.1007/s00216-007-1790-1>.
- Buades, A., Coll, B., and Morel, J.-M. A Non-Local Algorithm for Image Denoising. volume 2, pp. 60–65, San Diego, CA, USA, 2005a. IEEE. ISBN 978-0-7695-2372-9. doi: 10.1109/CVPR.2005.38. URL <http://ieeexplore.ieee.org/document/1467423/>.
- Buades, A., Coll, B., and Morel, J. M. A Review of Image Denoising Algorithms, with a New One. *Multiscale Modeling & Simulation*, 4(2):490–530, January 2005b. ISSN 1540-3459, 1540-3467. doi: 10.1137/040616024. URL <http://epubs.siam.org/doi/10.1137/040616024>.
- Chang, S. G., Yu, B., and Vetterli, M. Adaptive wavelet thresholding for image denoising and compression. *IEEE transactions on image processing*, 9(9):1532–1546, 2000.
- Dabov, K., Foi, A., Katkovnik, V., and Egiazarian, K. Image Denoising by Sparse 3-D Transform-Domain Collaborative Filtering. *IEEE Transactions on Image Processing*, 16(8):2080–2095, August 2007. ISSN 1057-7149. doi: 10.1109/TIP.2007.901238.
- Ehret, T., Davy, A., Facciolo, G., Morel, J.-M., and Arias, P. Model-blind Video Denoising Via Frame-to-frame Training. *arXiv:1811.12766 [cs]*, November 2018. URL <http://arxiv.org/abs/1811.12766>. arXiv: 1811.12766.
- Elad, M. and Aharon, M. Image Denoising Via Sparse and Redundant Representations Over Learned Dictionaries. *IEEE Transactions on Image Processing*, 15(12): 3736–3745, December 2006. ISSN 1057-7149. doi: 10.1109/TIP.2006.881969. URL <http://ieeexplore.ieee.org/document/4011956/>.
- Gallinari, P., Lecun, Y., Thiria, S., and Soulie, F. Memoires associatives distribuees: Une comparaison (Distributed associative memories: A comparison). *Proceedings of COGNITIVA 87, Paris, La Villette, May 1987*, 1987.
- Krull, A., Buchholz, T.-O., and Jug, F. Noise2void - Learning Denoising from Single Noisy Images. *arXiv:1811.10980 [cs]*, November 2018. URL <http://arxiv.org/abs/1811.10980>. arXiv: 1811.10980.
- Lebrun, M. An Analysis and Implementation of the BM3d Image Denoising Method. *Image Processing On Line*, 2:175–213, August 2012. ISSN 2105-1232. doi: 10.5201/ipol.2012.1-bm3d. URL <http://www.ipol.im/pub/art/2012/1-bm3d/>.
- LeCun, Y., Bottou, L., Bengio, Y., and Haffner, P. Gradient-based learning applied to document recognition. *Proceedings of the IEEE*, 86(11):2278–2324, 1998.
- Lehtinen, J., Munkberg, J., Hasselgren, J., Laine, S., Karras, T., Aittala, M., and Aila, T. Noise2noise: Learning Image Restoration without Clean Data. pp. 10, 2018.
- Metzler, C. A., Mousavi, A., Heckel, R., and Baraniuk, R. G. Unsupervised Learning with Stein’s Unbiased Risk Estimator. *arXiv:1805.10531 [cs, stat]*, May 2018. URL <http://arxiv.org/abs/1805.10531>. arXiv: 1805.10531.
- Milo, R., Jorgensen, P., Moran, U., Weber, G., and Springer, M. BioNumbersthe database of key numbers in molecular and cell biology. *Nucleic Acids Research*, 38 (suppl\_1):D750–D753, January 2010. ISSN 0305-1048, 1362-4962. doi: 10.1093/nar/gkp889. URL <https://academic.oup.com/nar/article-lookup/doi/10.1093/nar/gkp889>.
- Murphy, K. P. *Machine learning: a probabilistic perspective*. Adaptive computation and machine learning series. MIT Press, Cambridge, MA, 2012. ISBN 978-0-262-01802-9.
- Owen, A. B. and Perry, P. O. Bi-cross-validation of the SVD and the nonnegative matrix factorization. *The Annals of Applied Statistics*, 3(2):564–594, June 2009. ISSN 1932-6157. doi: 10.1214/08-AOAS227. URL <http://projecteuclid.org/euclid.aoas/1245676186>.
- Owen, A. B., Wang, J., and others. Bi-cross-validation for factor analysis. *Statistical Science*, 31(1):119–139, 2016.
- Papayan, V., Romano, Y., Sulam, J., and Elad, M. Convolutional Dictionary Learning via Local Processing. *arXiv:1705.03239 [cs]*, May 2017. URL <http://arxiv.org/abs/1705.03239>.
- Paul, F., Arkin, Y., Giladi, A., Jaitin, D., Kenigsberg, E., Keren-Shaul, H., Winter, D., Lara-Astiaso, D., Gury, M., Weiner, A., David, E., Cohen, N., Lauridsen, F., Haas, S., Schlitzer, A., Mildner, A., Ginhoux, F., Jung, S., Trumpp, A., Porse, B., Tanay, A., and Amit, I. Transcriptional Heterogeneity and Lineage Commitment in

- Myeloid Progenitors. *Cell*, 163(7):1663–1677, December 2015. ISSN 00928674. doi: 10.1016/j.cell.2015.11.013. URL <https://linkinghub.elsevier.com/retrieve/pii/S0092867415014932>.
- Pennebaker, W. B. and Mitchell, J. L. *JPEG still image data compression standard*. Van Nostrand Reinhold, New York, 1992. ISBN 978-0-442-01272-4.
- Ronneberger, O., Fischer, P., and Brox, T. U-Net: Convolutional Networks for Biomedical Image Segmentation. *arXiv:1505.04597 [cs]*, May 2015. URL <http://arxiv.org/abs/1505.04597>. arXiv: 1505.04597.
- Tripathi, S., Lipton, Z. C., and Nguyen, T. Q. Correction by Projection: Denoising Images with Generative Adversarial Networks. *arXiv:1803.04477 [cs]*, March 2018. URL <http://arxiv.org/abs/1803.04477>.
- Ulyanov, D., Vedaldi, A., and Lempitsky, V. Deep Image Prior. *arXiv:1711.10925 [cs, stat]*, November 2017. URL <http://arxiv.org/abs/1711.10925>. arXiv: 1711.10925.
- Vincent, P., Larochelle, H., Lajoie, I., Bengio, Y., and Manzagol, P.-A. Stacked denoising autoencoders: Learning useful representations in a deep network with a local denoising criterion. *Journal of machine learning research*, 11(Dec):3371–3408, 2010.
- Weigert, M., Schmidt, U., Boothe, T., Mller, A., Dibrov, A., Jain, A., Wilhelm, B., Schmidt, D., Broaddus, C., Culley, S., Rocha-Martins, M., Segovia-Miranda, F., Norden, C., Henriques, R., Zerial, M., Solimena, M., Rink, J., Tomancak, P., Royer, L., Jug, F., and Myers, E. W. Content-Aware Image Restoration: Pushing the Limits of Fluorescence Microscopy. July 2018. doi: 10.1101/236463. URL <http://biorxiv.org/lookup/doi/10.1101/236463>.
- Zhang, K., Zuo, W., Chen, Y., Meng, D., and Zhang, L. Beyond a Gaussian Denoiser: Residual Learning of Deep CNN for Image Denoising. *IEEE Transactions on Image Processing*, 26(7):3142–3155, July 2017. ISSN 1057-7149, 1941-0042. doi: 10.1109/TIP.2017.2662206. URL <http://ieeexplore.ieee.org/document/7839189/>.
- Zhussip, M., Soltanayev, S., and Chun, S. Y. Training deep learning based image denoisers from undersampled measurements without ground truth and without image prior. *arXiv:1806.00961 [cs]*, June 2018. URL <http://arxiv.org/abs/1806.00961>. arXiv: 1806.00961.

---

# Supplement to Noise2Self: Blind Denoising by Self-Supervision

---

## 1. Notation

For a variables  $x \in \mathbb{R}^m$  and  $J \subset \{1, \dots, m\}$ , we write  $x_J$  for the restriction of  $x$  to the coordinates in  $J$  and  $x_{J^c}$  for the restriction of  $x$  to the coordinates in  $J^c$ . If  $f: \mathbb{R}^m \rightarrow \mathbb{R}^m$  is a function, we write  $f(x)_J$  for the restriction of  $f(x)$  to the coordinates in  $J$ .

A partition  $\mathcal{J}$  of a set  $X$  is a set of disjoint subsets of  $X$  whose union is all of  $X$ .

When  $J = \{j\}$  is a singleton, we write  $x_{-j}$  for  $x_{J^c}$ , the restriction of  $x$  to the coordinates not equal to  $j$ .

## 2. Gaussian Processes

Let  $x$  and  $y$  be random variables. Then the estimator of  $y$  from  $x$  minimizing the expected mean-square error (MSE) is  $x \mapsto \mathbb{E}[y|x]$ . The expected MSE of that estimator is simply the variance of  $y|x$ :

$$\mathbb{E}_x \|y - \mathbb{E}[y|x]\|^2 = \mathbb{E}_x \text{Var}(y|x).$$

If  $x$  and  $y$  are jointly multivariate normal, then the right-hand-side depends only on the covariance matrix  $\Sigma$ . If

$$\Sigma = \begin{pmatrix} \Sigma_{xx} & \Sigma_{yx} \\ \Sigma_{xy} & \Sigma_{yy} \end{pmatrix},$$

then then right-hand-side is in fact a constant independent of  $x$ :

$$\text{Var}(y|x) = \Sigma_{yy} - \Sigma_{yx}\Sigma_{xx}^{-1}\Sigma_{xy}.$$

(See Chapter 4 of (Murphy, 2012).)

**Lemma 1.** *Let  $\Sigma$  be a symmetric, positive semi-definite matrix with block structure*

$$\Sigma = \begin{pmatrix} \Sigma_{11} & \Sigma_{12} \\ \Sigma_{21} & \Sigma_{22} \end{pmatrix}.$$

Then

$$\Sigma_{11} \succeq \Sigma_{12}\Sigma_{22}^{-1}\Sigma_{21}.$$

*Proof.* Since  $\Sigma$  is PSD, we may factorize it as a product  $X^T X$  for some matrix  $X$ . (For example, take the spectral decomposition  $\Sigma = V^T \Lambda V$ , with  $\Lambda$  the diagonal matrix of

eigenvalues, all of which are nonnegative since  $\Sigma$  is PSD and  $V$  the matrix of eigenvectors. Set  $X = \Lambda^{1/2}V$ .)

Write

$$X = \begin{pmatrix} X_1 & X_2 \end{pmatrix},$$

so that  $\Sigma_{ij} = X_i^T X_j$ . If  $\pi_{X_2}$  is the projection operator onto the column-span of  $X_2$ , then

$$I \succeq \pi_{X_2} = X_2(X_2^T X_2)^{-1}X_2^T.$$

Multiplying on the left and right by  $X_1^T$  and  $X_1$  yields

$$\begin{aligned} X_1^T X_1 &\succeq X_1^T X_2 (X_2^T X_2)^{-1} X_2^T X_1 \\ \Sigma_{11} &\succeq \Sigma_{12} \Sigma_{22}^{-1} \Sigma_{21}, \end{aligned}$$

where the second line follows by grouping terms in the first.  $\square$

**Lemma 2.** *Let  $x, y$  be random variables and let  $x^G$  and  $y^G$  be Gaussian random variables with the same covariance matrix. Then*

$$\mathbb{E}_x \|y - \mathbb{E}[y|x]\|^2 \leq \mathbb{E}_{x^G} \|y^G - \mathbb{E}[y^G|x^G]\|^2.$$

*Proof.* These are in fact the expected variances of the conditional variables:

$$\mathbb{E} \|y - \mathbb{E}[y|x]\|^2 = \mathbb{E}_x \mathbb{E}_{y|x} \|y - \mathbb{E}[y|x]\|^2 = \mathbb{E}_x \text{Var}[y|x].$$

Using the formula above for the Gaussian process MSE, we now need to show that

$$\mathbb{E}_x \text{Var}[y|x] \leq \Sigma_{yy} - \Sigma_{yx}\Sigma_{xx}^{-1}\Sigma_{xy}.$$

By the law of total variance,

$$\text{Var}(y) = \text{Var}_x(\mathbb{E}[y|x]) + \mathbb{E}_x \text{Var}(y|x).$$

So it suffices to show that

$$\text{Var}_x(\mathbb{E}[y|x]) \geq \Sigma_{yx} \Sigma_{xx}^{-1} \Sigma_{xy}.$$

Without loss of generality, we set  $\mathbb{E}x = \mathbb{E}y = 0$ . We compute the covariance of  $x$  with  $\mathbb{E}[y|x]$ . We have

$$\begin{aligned} \text{Cov}(x, \mathbb{E}[y|x]) &= \mathbb{E}_x [x \cdot \mathbb{E}[y|x]] \\ &= \mathbb{E}_x [\mathbb{E}[xy|x]] \\ &= \mathbb{E}_x [\mathbb{E}[xy]] \\ &= \mathbb{E}[xy] \\ &= \text{Cov}(x, y) \end{aligned}$$

The statement follows from an application of Lemma 1 to the covariance matrix of  $x$  and  $\mathbb{E}[y|x]$ .  $\square$

**Proposition 1.** *Let  $x, y$  be random variables and let  $x^G$  and  $y^G$  be Gaussian random variables with the same covariance matrix. Let  $f_{\mathcal{J}}^*$  and  $f_{\mathcal{J}}^{*,G}$  be the corresponding optimal  $\mathcal{J}$ -invariant predictors. Then*

$$\mathbb{E} \|y - f_{\mathcal{J}}^*(x)\|^2 \leq \mathbb{E} \|y - f_{\mathcal{J}}^{*,G}(x)\|^2.$$

*Proof.* We first reduce the statement to unconstrained optimization, noting that

$$f_{\mathcal{J}}^*(x)_j = \mathbb{E}y_j | x_{J^c}.$$

The statement follows from Lemma 2 applied to  $y_j, x_{J^c}$ .  $\square$

### 3. Masking

In this section, we discuss approaches to modifying the input to a neural net or other function  $f$  to create a  $\mathcal{J}$ -invariant function.

The basic idea is to choose some interpolation function  $s(x)$  and then define  $g$  by

$$g(x)_J := f(\mathbf{1}_J \cdot s(x) + \mathbf{1}_{J^c} \cdot x)_J,$$

where  $\mathbf{1}_J$  is the indicator function of the set  $J$ .

In Section 3 of the paper, on calibration,  $s$  is given by a local average, not containing the center. Explicitly, it is convolution with the kernel

$$\begin{pmatrix} 0 & 0.25 & 0 \\ 0.25 & 0 & 0.25 \\ 0 & 0.25 & 0 \end{pmatrix}.$$

We also considered setting each entry of  $s(x)$  to a random variable uniform on  $[0, 1]$ . This produces a random  $\mathcal{J}$ -invariant function, ie, a distribution  $g(x)$  whose marginal  $g(x)_J$  does not depend on  $x_J$ .

#### 3.1. Uniform Pixel Selection

In Krull et. al., the authors propose masking procedures that estimate a local distribution  $q(x)$  in the neighborhood of a pixel and then replace that pixel with a sample from the distribution. Because the value at that pixel is used to estimate the distribution, information about it leaks through and the resulting random functions are not genuinely  $J$ -invariant.

For example, they propose a method called Uniform Pixel Selection (UPS) to train a neural net to predict  $x_j$  from  $\text{UPS}_j(x)$ , where  $\text{UPS}_j$  is the random function replacing the  $j^{\text{th}}$  entry of  $x$  with the value of at a pixel  $k$  chosen uniformly at random from the  $r \times r$  neighborhood centered at  $j$  (Krull et al., 2018).

Write  $\iota_{jk}(x)$  is the vector  $x$  with the value  $x_j$  replaced by  $x_k$ .

The function  $f^*$  minimizing the self-supervised loss

$$\mathbb{E}_x \|f(\text{UPS}_j(x))_j - x_j\|^2$$

satisfies

$$\begin{aligned} f^*(x)_j &= \mathbb{E}_x [x_j | \text{UPS}_j(x)] \\ &= \mathbb{E}_x \mathbb{E}_k [x_j | \iota_{jk}(x)] \\ &= \frac{1}{r^2} \sum_k \mathbb{E} [x_j | \iota_{jk}(x)] \\ &= \frac{1}{r^2} \mathbb{E} [x_j | \iota_{jj}(x)] + \frac{1}{r^2} \sum_{k \neq j} \mathbb{E} [x_j | \iota_{jk}(x)] \\ &= \frac{1}{r^2} x_j + \frac{1}{r^2} \sum_{k \neq j} \mathbb{E} [x_j | x_{-j}] \\ &= \frac{1}{r^2} x_j + \left(1 - \frac{1}{r^2}\right) f_{\mathcal{J}}^*(x)_j, \end{aligned}$$

where  $f_{\mathcal{J}}^*(x)_j = \mathbb{E}[x_j | x_{-j}]$  is the optimum of the self-supervised loss among  $\mathcal{J}$ -invariant functions.

This means that training using UPS masking can, given sufficient data and a sufficiently expressive network, produce a linear combination of the noisy input and the Noise2Self optimum. The smaller the region used for selecting the pixel, the larger the contribution of the noise will be. In practice, however, a convolutional neural net may not be able to learn to recognize when it was handed an interesting pixel  $x_j$  and

when it had been replaced (say by comparing the value at a pixel in  $\text{UPS}_j(x)$  to each of its neighbors).

One attractive feature of UPS is that it keeps the same per-pixel data distribution as the input. If, for example, the input is binary, then local averaging and random uniform replacements will both be substantial deviations. This may regularize the behavior of the network, making it more sensible to pass in an entire copy of  $x$  to the trained network later, rather than iteratively masking it.

We suggest a simple modification: exclude the value of  $x_j$  when estimating the local distribution. For example, replace it with a random neighbor.

### 3.2. Linear Combinations

In this section we note that if  $f$  is  $\mathcal{J}$ -invariant, then  $f(x)_j$  and  $x_j$  give two uncorrelated estimators of  $y_j$  for any coordinate  $j$ . Here we investigate the effect of taking a linear combination of them.

Given two uncorrelated and unbiased estimators  $u$  and  $v$  of some quantity  $y$ , we may form a linear combination:

$$w_\lambda = \lambda u + (1 - \lambda)v.$$

The variance of this estimator is

$$\lambda^2 U + (1 - \lambda)^2 V,$$

where  $U$  and  $V$  are the variances of  $u$  and  $v$  respectively. This expression is minimized at

$$\lambda = V/(U + V).$$

The variance of the mixed estimator  $w_\lambda$  is  $UV/(U + V) = V \frac{1}{1+V/U}$ . When the variance of  $v$  is much lower than that of  $u$ , we just get  $V$  out, but when they are the same the variance is exactly halved. Note that this is monotonic in  $V$ , so if estimators  $v_1, \dots, v_n$  are being compared, their rank will not change after the original signal is mixed in. In terms of PSNR, the new value is

$$\begin{aligned} \text{PSNR}(w_\lambda, y) &= 10 * \log_{10} \left( \frac{1 + V/U}{V} \right) \\ &= \text{PSNR}(V) + 10 * \log_{10}(1 + V/U) \\ &\approx \text{PSNR}(V) + \frac{10}{\log_{10}(e)} \left( \frac{V}{U} - \frac{1}{2} \frac{V^2}{U^2} \right) \\ &\approx \text{PSNR}(V) + 4.3 * \frac{V}{U} \end{aligned}$$

If we fix  $y$ , then  $x_j$  and  $\mathbb{E}[y_j|x_{-j}]$  are both independent estimators of  $y_j$ , so the above reasoning applies. Note that the loss itself is the variance of  $x_j|x_{-j}$ , whose two components are the variance of  $x_j|y_j$  and the variance of  $y_j|x_{-j}$ .

The optimal value of  $\lambda$ , then, is given by the variance of the noise divided by the value of the self-supervised loss. For example the function  $f$  reduces the noise by a factor of 10 (ie, the variance of  $y_j|x_{-j}$  is a tenth of the variance of  $x_j|y_j$ ), then  $\lambda^* = 1/11$  and the linear combination has a PSNR 0.43 higher than that of  $f$  alone.

## 4. Calibrating Traditional Denoising Methods

The image denoising methods were all demonstrated on the full camera image included in the `scikit-image` library for python (van der Walt et al., 2014). An inset from that image was displayed in the figures.

We also used the `scikit-image` implementations of the median filter, wavelet denoiser, and NL-means. The noise standard deviation was 0.1 on a  $[0, 1]$  scale.

In addition to the calibration plots for the median filter in the text, we show the same for the wavelet and NL-means denoisers in Supp. Figure 1.

## 5. Neural Net Examples

### 5.1. Datasets: Hànzì, CellNet, ImageNet

**Hànzì** We constructed a dataset of 13029 Chinese characters (hànzì) rendered as white on black 64x64 images (image intensity within  $[0, 1]$ ), and applied to each one substantial Gaussian ( $\mu = 0, \sigma = 0.7$ ) and Bernoulli (half pixels blacked out) noise. Each Chinese character appears 6 times in the whole dataset of 78174 images. We then split this dataset in a training and test set (90% versus 10%).

**CellNet** We constructed a dataset of 34630 image tiles (128x128) obtained by random partitioning of a large collection of single channel fluorescence microscopy images of cultured cells. These images were downloaded from the *Broad Bioimage Benchmark Collection* (Ljosa et al., 2012). Before cropping, we first gently denoise the images using the non-local means algorithm. We do so in order to remove a very low and nearly imperceptible amount of noise already present in these images – indeed, the images have an excellent signal-to-noise ratio to start from. Next, we use a rich noise model to simulate typical noise on sCMOS scientific cameras. This noise model consists of: (i) spatially variant gain noise per pixel, (ii) Poisson noise, (iii) Cauchy distributed additive noise. We choose parameters so as to obtain a very aggressive noise regime.

**ImageNet** In order to generate a large collection of natural image tiles, we downloaded the *ImageNet LSVRC 2013 Vali-*

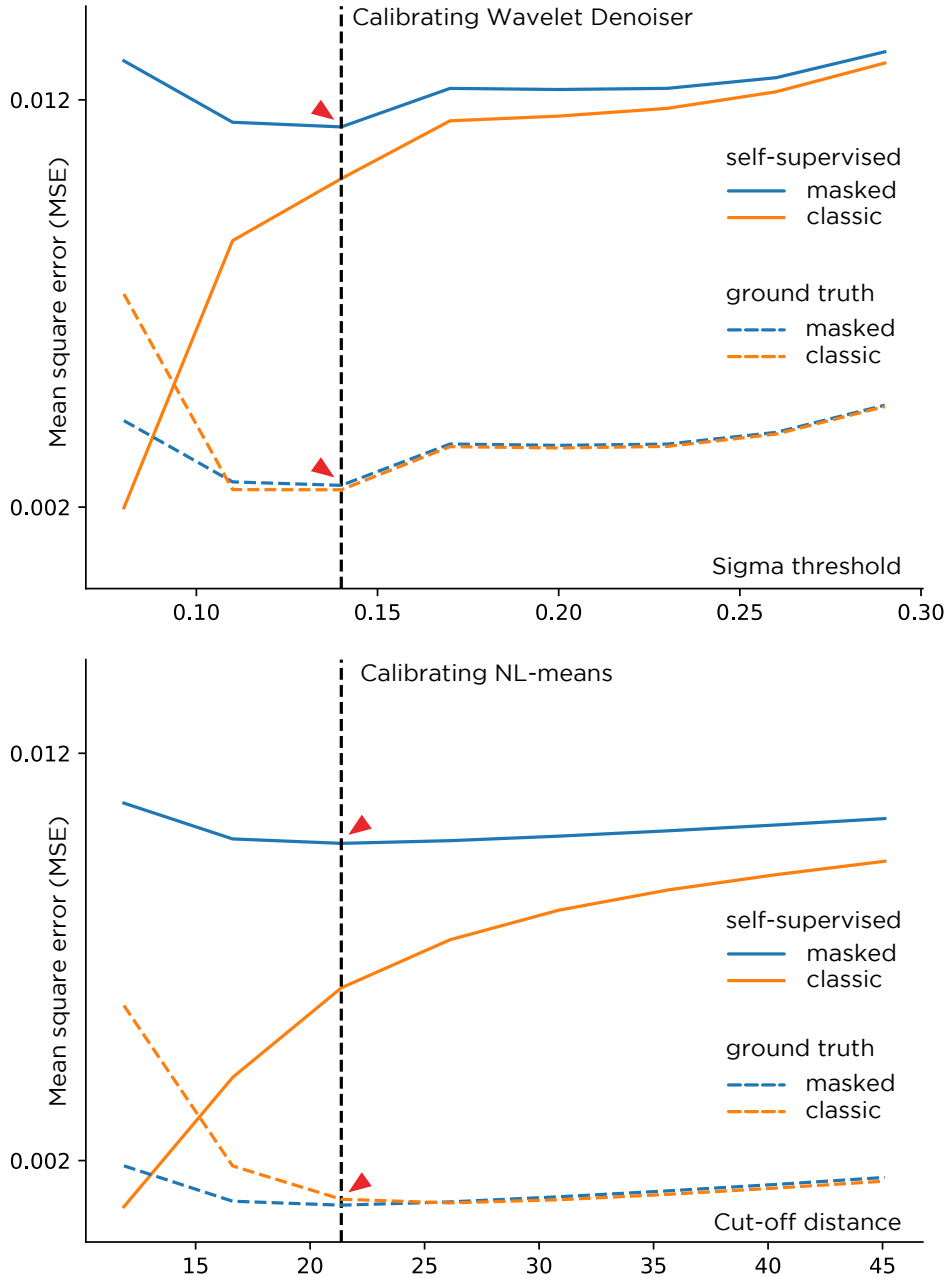


Figure 1. Calibrating a wavelet filter and Non-local means without ground truth. The optimal parameter for  $\mathcal{J}$ -invariant (masked) versions can be read off (red arrows) from the self-supervised loss.

dition Set consisting of 20121 RGB images – typically photographs. From these images we generated 60000 cropped images of dimension 128x128 with each RGB value within [0, 255]. These images were mistreated by the strong combination of Poisson ( $\lambda = 30$ ), Gaussian ( $\sigma = 80$ ), and Bernoulli noise ( $p = 0.2$ ). In the case of Bernoulli noise, each pixel channel (R, G, or B) has probability  $p$  of being dark or hot, i.e. set to the value 0 or 255.

### 5.2. Architecture

We use a UNet architecture modelled after (Ronneberger et al., 2015). The network has an hourglass shape with skip connections between layers of the same scale. Each convolutional block consists of two convolutional layers with 3x3 filters followed by an InstanceNorm. The number of channels is [32, 64, 128, 256]. Downsampling uses strided

convolutions and upsampling uses transposed convolutions. The network is implemented in PyTorch (Paszke et al., 2017) and the code is also included in the supplement.

### 5.3. Training

We convert a neural net  $f_\theta$  into a random  $\mathcal{J}$ -invariant function:

$$\sum_{J \in \mathcal{J}} \mathbf{1}_J \cdot f_\theta(\mathbf{1}_{J^c} \cdot x_J + \mathbf{1}_J \cdot u) \quad (1)$$

where  $u$  is a vector of random numbers distributed uniformly on  $[0, 1]$ . To speed up training, we only compute the coordinates for one  $J$  per pass, and that  $J$  is chosen randomly for each batch with density  $1/25$ . The loss is restricted to those coordinates.

We train with a batch size of 64 for **Hànzì** and **CellNet** and a batch size of 32 for **ImageNet**.

We train for 50 epochs for **CellNet**, 30 epochs for **Hànzì** and 1 epoch for **ImageNet**.

### 5.4. Inference

We considered two approaches for inference. In the first, we consider a partition  $\mathcal{J}$  containing 25 sets and apply Equation (1) to produce a genuinely  $\mathcal{J}$ -invariant function. This requires  $|\mathcal{J}|$  applications of the network.

In the second, we just apply the trained network to the full noisy data. This will include the information from  $x_j$  in the prediction  $f_\theta(x)_j$ . While the information in this pixel was entirely redundant during training, some regularization induced by the convolutional structure of the net and the training procedure may have caused it to learn a function which uses that information in a sensible way. Indeed, on our three datasets, the direct application was about 0.5 dB better than the  $\mathcal{J}$ -independent version.

### 5.5. Evaluation

We evaluated each reconstruction method using the Peak Signal-to-Noise Ratio (PSNR). For two images with range  $[0, 1]$ , this is a log-transformation of the mean-squared error:

$$\text{PSNR}(x, y) = 10 * \log_{10}(1 / \|x - y\|^2).$$

Because of clipping, the noise on the image datasets is not conditionally mean-zero. (Any noise on a pixel with intensity 1, for example, must be negative.) This induces a bias:  $\mathbb{E}[x|y]$  is shrunk slightly towards the mean intensity. For methods trained with clean targets, like Noise2Truth and DnCNN, this effect doesn't matter; the network can learn to produce the correct value. The outputs of the blind methods

like Noise2Noise, Noise2Self, NL-means, and BM3D, will exhibit this shrinkage. To make up for this difference, we rescale the outputs of all methods to match the mean and variance of the ground truth.

We compute the PSNR for fully reconstructed images on hold-out test sets which were not part of the training or validation procedure.

## 6. Single-Cell Gene Expression

The lossy capture and sequencing process producing single-cell gene expression can be expressed as a Poisson distribution<sup>1</sup>. A given cell has a density  $\lambda = (\lambda_1, \dots, \lambda_m)$  over genes  $i \in \{1, \dots, m\}$ , with  $\sum_i \lambda_i = 1$ . If we sample  $N$  molecules, we get a multinomial distribution which can be approximated as  $x_i \sim \text{Poisson}(N\lambda_i)$ .

While one would like to model molecular counts directly, the large dynamic range of gene expression (about 5 orders of magnitude) makes linear models difficult to fit directly. Instead, one typically introduces a normalized variable  $z$ , for example

$$z_i = \rho(N_0 * x_i / N),$$

where  $N = \sum_i x_i$  is the total number of molecules in a given cell,  $N_0$  is a normalizing constant, and  $\rho$  is some nonlinearity. Common values for  $\rho$  include  $x \mapsto \sqrt{x}$  and  $x \mapsto \log(1 + x)$ .

Our analysis of the Paul et al. dataset (Paul et al., 2015) follows one from the tutorial for a diffusion-based denoiser called MAGIC, and we use the `scprep` package to perform normalization (Van Dijk et al., 2018). In the language above,  $N_0$  is the median of the total molecule count per cell and  $\rho$  is square root.

Because we work on the normalized variable  $z$ , the optimal denoiser would predict

$$\mathbb{E}[z_i | \lambda] \approx \mathbb{E}_{x_i \sim \text{Poisson } N\lambda_i} \sqrt{x_i} \sqrt{N_0 / N}.$$

This function of  $\lambda_i$  is positive, monotonic and maps 0 to 0, so it is directionally informative. Since expectations do not commute with nonlinear functions, inverting it would not produce an unbiased estimate of  $\lambda_i$ . Nevertheless, it provides a quantitative estimate of gene expression which is well-adapted to the large dynamic range.

<sup>1</sup> While the polymerase chain reaction (PCR) used to amplify the molecules for sequencing would introduce random multiplicative distortions, many modern datasets introduce unique molecular identifiers (UMIs), barcodes attached to each molecule before amplification which can be used to deduplicate reads from the same original molecule.

## References

- 275 Krull, A., Buchholz, T.-O., and Jug, F. Noise2void  
276 - Learning Denoising from Single Noisy Images.  
277 *arXiv:1811.10980 [cs]*, November 2018. URL  
278 <http://arxiv.org/abs/1811.10980>. arXiv:  
279 1811.10980.  
280  
281
- 282 Ljosa, V., Sokolnicki, K. L., and Carpenter, A. E. Annotated  
283 high-throughput microscopy image sets for validation.  
284 *Nature Methods*, 9(7):637–637, July 2012. ISSN 1548-  
285 7091, 1548-7105. doi: 10.1038/nmeth.2083. URL [http:  
286 //www.nature.com/articles/nmeth.2083](http://www.nature.com/articles/nmeth.2083).  
287
- 288 Murphy, K. P. *Machine learning: a probabilistic perspective*.  
289 Adaptive computation and machine learning series. MIT  
290 Press, Cambridge, MA, 2012. ISBN 978-0-262-01802-9.  
291
- 292 Paszke, A., Gross, S., Chintala, S., Chanan, G., Yang, E.,  
293 DeVito, Z., Lin, Z., Desmaison, A., Antiga, L., and Lerer,  
294 A. Automatic differentiation in PyTorch. In *NIPS-W*,  
295 2017.
- 296 Paul, F., Arkin, Y., Giladi, A., Jaitin, D., Kenigsberg, E.,  
297 Keren-Shaul, H., Winter, D., Lara-Astiaso, D., Gury, M.,  
298 Weiner, A., David, E., Cohen, N., Lauridsen, F., Haas,  
299 S., Schlitzer, A., Mildner, A., Ginhoux, F., Jung, S.,  
300 Trumpp, A., Porse, B., Tanay, A., and Amit, I. Tran-  
301 scriptional Heterogeneity and Lineage Commitment in  
302 Myeloid Progenitors. *Cell*, 163(7):1663–1677, Decem-  
303 ber 2015. ISSN 00928674. doi: 10.1016/j.cell.2015.  
304 11.013. URL [https://linkinghub.elsevier.  
305 com/retrieve/pii/S0092867415014932](https://linkinghub.elsevier.com/retrieve/pii/S0092867415014932).  
306
- 307 Ronneberger, O., Fischer, P., and Brox, T. U-Net: Con-  
308 volutional Networks for Biomedical Image Segmen-  
309 tation. *arXiv:1505.04597 [cs]*, May 2015. URL  
310 <http://arxiv.org/abs/1505.04597>. arXiv:  
311 1505.04597.
- 312 van der Walt, S., Schnberger, J. L., Nunez-Iglesias, J.,  
313 Boulogne, F., Warner, J. D., Yager, N., Gouillart, E.,  
314 Yu, T., and contributors, t. s.-i. scikit-image: image  
315 processing in Python. *PeerJ*, 2:e453, 2014. ISSN  
316 2167-8359. doi: 10.7717/peerj.453. URL [https:  
317 //doi.org/10.7717/peerj.453](https://doi.org/10.7717/peerj.453).  
318
- 319 Van Dijk, D., Sharma, R., Nainys, J., Yim, K., Kathail, P.,  
320 Carr, A., Burdziak, C., Moon, K. R., Chaffer, C. L., Pat-  
321 tabiraman, D., and others. Recovering Gene Interactions  
322 from Single-Cell Data Using Data Diffusion. 2018.  
323  
324  
325  
326  
327  
328  
329